Role of functionality in two-component signal transduction: A stochastic study

Alok Kumar Maity,[1] Arnab Bandyopadhyay,[2] Pinaki Chaudhury,[1,*] and Suman K. Banik[2,†]
[1]*Department of Chemistry, University of Calcutta, 92 A P C Road, Kolkata 700 009, India*
[2]*Department of Chemistry, Bose Institute, 93/1 A P C Road, Kolkata 700 009, India*
(Received 2 July 2013; revised manuscript received 11 December 2013; published 24 March 2014)

We present a stochastic formalism for signal transduction processes in a bacterial two-component system. Using elementary mass action kinetics, the proposed model takes care of signal transduction in terms of a phosphotransfer mechanism between the cognate partners of a two-component system, viz., the sensor kinase and the response regulator. Based on the difference in functionality of the sensor kinase, the noisy phosphotransfer mechanism has been studied for monofunctional and bifunctional two-component systems using the formalism of the linear noise approximation. Steady-state analysis of both models quantifies different physically realizable quantities, e.g., the variance, the Fano factor (variance/mean), and mutual information. The resultant data reveal that both systems reliably transfer information of extracellular environment under low external stimulus and in a high-kinase-and-phosphatase regime. We extend our analysis further by studying the role of the two-component system in downstream gene regulation.

DOI: 10.1103/PhysRevE.89.032713 PACS number(s): 87.18.Mp, 05.40.−a, 87.18.Tt, 87.18.Vf

I. INTRODUCTION

In response to the changes made in the extracellular environment, living systems adapt themselves by coordinated regulation of intracellular machinery composed of several interacting components [1–3]. In the bacterial kingdom, such adaptation is achieved by a group of highly specialized motifs, commonly known as a two-component system (TCS) [4–6]. Composed of membrane-bound sensor kinase and a cytoplasmic response regulator, a TCS detects changes made in the environment and, in response, controls expression and/or repression of one or several downstream genes (target genes other than the operon). In the presence of an external stimulus, autophosphorylation takes place in the conserved histidine residue of the sensor kinase. The phosphate group is then transferred to its cognate partner, the response regulator, containing the conserved aspartate domain. When phosphorylated, the response regulator regulates one or several downstream genes, as well as its own operon. For example, in *Mycobacterium tuberculosis*, the response regulator MprA gets phosphorylated by its cognate sensor MprB in the presence of the signal and exerts a positive feedback on its own operon, *mprAB* [7]. In addition to being the source of a phosphate group, sensor kinase sometimes can dephosphorylate the phosphate group from a response regulator by acting as phosphatase. This combined kinase and phosphatase activity of the sensor kinase makes the TCS bifunctional [5,6,8,9]. Due to the opposing (kinase and phosphatase) effect of sensor kinase on the response regulator, bifunctional systems have been placed in a broad category of functional motifs known as *paradoxical components* [10,11]. In certain TCSs, the role of a sensor as a phosphatase is absent, and the job of dephosphorylation is done by an auxiliary protein (phosphatase), thus making the TCS monofunctional [5,6].

Depending on the nature of the extracellular stimulus, a single bacterium may utilize different types of TCSs with highly specific functionality to transduce the changes made in the surroundings. To sense and adapt appropriately, a single bacterium may contain both monofunctional and bifunctional TCSs [5,6]. For example, the *Escherichia coli* chemotaxis system has CheA/CheY TCS that responds to changes in the chemical gradient in the surrounding area where the sensor kinase CheA is monofunctional in nature (acts as kinase only) and the role of phosphatase is played by CheZ, which is not a part of the TCS. On the other hand, EnvZ/OmpR TCS in *E. coli* responds to changes in the osmolarity of the environment where the sensor kinase EnvZ plays a bifunctional role (acts as a kinase as well as a phosphatase). One of the advantages of a bifunctional system over a monofunctional one is that it takes care of *input-output robustness* [12]. Due to its architecture, the output level of the phosphorylated response regulator in a bifunctional system depends only on the input stimulus and is independent of other system components. On the other hand, such a robustness criterion does not remain valid in a monofunctional system. Thus, in the latter case, in addition to the input stimulus, the output level depends also on the level of the phosphatase which acts on the phosphorylated response regulator.

When the aforesaid signal transduction processes are considered within the single-cell scenario, the role of fluctuations, cellular and/or extracellular, cannot be ruled out. Whether external or internal, such fluctuations not only affect the gene expression mechanism within a cell but also control the signal transduction processes involving post-translational modifications that are taking place within a noisy environment. With the advancement of experimental techniques that employ single-cell measurement, it is now possible to quantify different physically realizable quantities like the variance, the Fano factor (variance/mean), etc., of different cellular components [13–20]. In this light, it is thus worthwhile to develop a stochastic formalism to study signal transduction processes in bacterial TCSs, keeping in mind the difference in functionality of the sensor kinase. Although deterministic modeling of bacterial signal transduction machinery is known in the literature [7,12,21–24], few attempts have been made to study the same using a stochastic framework. In this

*pinakc@rediffmail.com
†Corresponding author: skbanik@jcbose.ac.in

connection, it is important to mention the theoretical modeling of bacterial two-component systems where stochastic kinetics has been used to study different phenotypic response (graded and all-or-none) [25,26]. In the present work, however, we have developed a mathematical formalism to study signal transduction processes in generic bacterial TCS. While developing the model, we have taken into account only the post-translational modification in terms of phosphorylation-dephosphorylation kinetics as the time scale of the phosphotransfer kinetics is faster than the synthesis and/or degradation time scale of the system components [21]. As mentioned earlier, the main role of a TCS is to transmit the information of changes in the extracellular environment reliably within the cell. In the proposed stochastic study, we compare information processing in a TCS with the monofunctional and the bifunctional properties of a sensor kinase. Combining both theoretical and numerical approaches, we show that for a fixed level of fluctuations due to stimulus, bifunctional TCS carries out a more reliable signal processing compared to monofunctional TCS.

The rest of the paper is organized as follows. In the next section, we develop the mathematical model to study the signal transduction mechanism in monofunctional and in bifunctional systems. Results of the model are discussed in Sec. III and the paper is concluded in Sec. IV.

II. THE MODEL

Following phosphotransfer kinetics depicted in Fig. 1 for both monofunctional and bifunctional systems, we have developed a mathematical model for noisy signal transduction in the present communication. In the presence of an external inducer I, sensor kinase S gets phosphorylated at the conserved histidine residue to form S_p. The phosphorylated sensor then transfers the phosphate group to its cognate response regulator R, forming R_p. It is important to note that the above-mentioned kinetics is common for both monofunctional and bifunctional systems. When it comes to removal of the phosphate group (dephosphorylation) from the response regulator, the two systems (monofunctional and bifunctional) behave differently. In the monofunctional system, the phosphate group from R_p is removed by a phosphatase P_h, whereas, in the bifunctional one, the phosphate group is removed by the unphosphorylated sensor S itself. Thus, in the monofunctional system, the sensor acts as a source of a phosphate group and, in the bifunctional system, the sensor acts as a sink in addition to being a source of the phosphate group. Considering the aforesaid interactions, the minimal kinetic steps for the phosphotransfer motif can be written as follows:

$$\xrightarrow{k_{sI}} I \xrightarrow{k_{dI}} \varnothing, \tag{1a}$$

$$S \underset{k_{dp}}{\overset{k_p I}{\rightleftharpoons}} S_p, \tag{1b}$$

$$S_p + R \xrightarrow{k_k} S + R_p, \tag{1c}$$

$$P_h + R_p \xrightarrow{k_{pm}} P_h + R, \tag{1d}$$

$$\xrightarrow{k_{sP_h}} P_h \xrightarrow{k_{dP_h}} \varnothing, \tag{1e}$$

$$S + R_p \xrightarrow{k_{pb}} S + R. \tag{1f}$$

In the above kinetic steps, Eq. (1a) refers to the synthesis and degradation of the external inducer I. Equation (1b) takes care of autophosphorylation and dephosphorylation of the sensor kinase. While modeling the autophosphorylation reaction, we have considered the signal I as a catalyst which helps to convert the sensor S to its phosphorylated form (S_p). However, the theoretical formalism developed earlier considered a more general framework for stochastic signaling through enzymatic futile cycles [27]. Equation (1c) considers the kinase reaction and Eq. (1d) considers the phosphatase activity of P_h towards R_p. It is important to mention that while writing the kinase and the phosphatase kinetics, we have considered a second-order bimolecular reaction scheme, although these reaction kinetics are generally written using Michaelis-Menten-type kinetics in the existing literature [7,21–24]. One of the advantages of using Michaelis-Menten kinetics is that it generates an ultrasensitive switch in a system [7,25,28–30] provided the network architecture generates substantial nonlinearity. However, the reason behind using the second-order bimolecular reaction scheme in the present work is that it makes our analytical calculation tractable, as shown in Sec. II A and Sec. II B. Since the auxiliary protein P_h behaves as an alternative source of phosphatase in the monofunctional system, it is worthwhile to consider its kinetics (synthesis and degradation) in the model. To this end, production and degradation of the phosphatase P_h has been taken care of by Eq. (1e). Finally, Eq. (1f) is due to the phosphatase activity of S towards R_p. Note that Eqs. (1a)–(1c) are common for both monofunctional and bifunctional systems. Equations (1d) and (1e) are exclusive for the monofunctional system and Eq. (1f) is solely for the bifunctional system. While writing the kinetic steps, we have mostly considered the post-translational modification for the sensor and response regulator. As mentioned earlier, we do not consider synthesis and degradation of the system

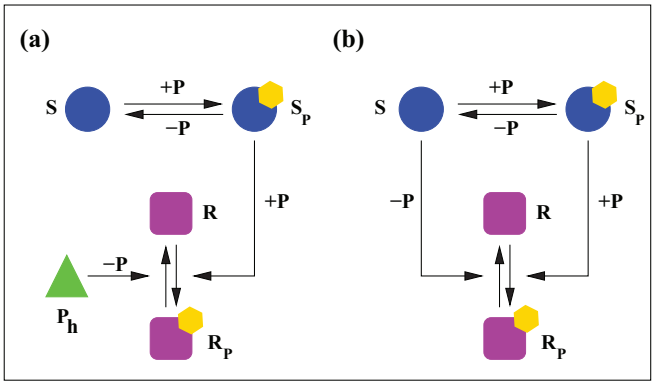

FIG. 1. (Color online) Schematic diagram of phosphotransfer motif in a (a) monofunctional and (b) bifunctional two-component system. S and S_p stand for the unphosphorylated and phosphorylated form of sensor kinase, respectively. Similarly, R and R_p stand for the unphosphorylated and phosphorylated forms of response regulator, respectively. P_h stands for phosphatase. $\pm P$ stand for the addition or removal of the phosphate group (shown by the orange hexagon). Note that in a monofunctional system sensor kinase acts as a source of a phosphate group, whereas, in a bifunctional system, it acts both as a source and sink for the phosphate group.

components (S and R) in the proposed model which keeps the total amount of sensor and response regulator constant, i.e., $S + S_p = S_T$ and $R + R_p = R_T$.

To understand the role of fluctuations prevalent due to the external inducer I and the intrinsic cellular noise affecting the phosphotransfer mechanism, we adopt the Langevin approach to define different physical quantities. The Langevin approach, within the purview of the linear noise approximation, is a valid approach provided fluctuations in the input signal are very small so one can linearize the resultant noise in the Langevin equation [13,30–32]. Such linearization also remains valid when the coarse-grained (steady-state) time scale is longer than the birth-death rate of system components. In addition, a large copy number of system components makes the approximation valid. Since, in TCSs, copy numbers of S and R are large, one can adopt the Langevin formalism to understand the stochastic signal transduction mechanism. Thus, the Langevin equation associated with the inducer kinetics is given by

$$\frac{dI}{dt} = k_{sI} - k_{dI} I + \xi_I, \tag{2}$$

where

$$\langle \xi_I(t) \rangle = 0, \quad \langle \xi_I(t) \xi_I(t+\tau) \rangle = 2k_{dI} \langle I \rangle \delta(\tau), \tag{3}$$

with $\langle I \rangle$ being the mean inducer level at steady state. It is important to note that Eqs. (2)–(3) are common for both monofunctional and bifunctional systems.

A. Monofunctional system

Considering the kinetic steps given by Eqs. (1b)–(1e) and fluctuations associated with them, the Langevin equations for S_p, R_p, and P_h for the monofunctional system can be written as

$$\frac{dS_p}{dt} = k_p(S_T - S_p)I - k_{dp} S_p - k_k S_p (R_T - R_p) + \xi_{S_p}, \tag{4a}$$

$$\frac{dR_p}{dt} = k_k S_p (R_T - R_p) - k_{pm} P_h R_p + \xi_{R_p}, \tag{4b}$$

$$\frac{dP_h}{dt} = k_{sP_h} - k_{dP_h} P_h + \xi_{P_h}. \tag{4c}$$

The additive noise terms ξ_{S_p}, ξ_{R_p}, and ξ_{P_h} take care of fluctuations in the copy number of S_p, R_p, and P_h, respectively. Using the concept of the linear noise approximation, the statistical properties of three fluctuating terms can be written as follows [33–35]:

$$\langle \xi_{S_p}(t) \xi_{S_p}(t+\tau) \rangle_m = 2k_p [S_T - \langle S_p \rangle_m] \langle I \rangle \delta(\tau), \tag{5a}$$

$$\langle \xi_{R_p}(t) \xi_{R_p}(t+\tau) \rangle_m = 2k_k \langle S_p \rangle_m [R_T - \langle R_p \rangle_m] \delta(\tau), \tag{5b}$$

$$\langle \xi_{P_h}(t) \xi_{P_h}(t+\tau) \rangle_m = 2k_{dP_h} \langle P_h \rangle \delta(\tau), \tag{5c}$$

with $\langle \xi_{S_p}(t) \rangle_m = \langle \xi_{R_p}(t) \rangle_m = \langle \xi_{P_h}(t) \rangle_m = 0$. In the above equations, $\langle S_p \rangle_m$ and $\langle R_p \rangle_m$ stand for the mean values of S_p and R_p at the steady state, respectively. Here, $\langle \cdots \rangle_m$ has been used to designate ensemble average for a monofunctional system. Furthermore, we consider that the noise terms ξ_{S_p} and ξ_{R_p} are correlated [30,36],

$$\langle \xi_{S_p}(t) \xi_{R_p}(t+\tau) \rangle_m = -k_k \langle S_p \rangle_m [R_T - \langle R_p \rangle_m] \delta(\tau). \tag{5d}$$

Linearizing Eq. (2) and Eqs. (4a)–(4c) around the mean value at steady state, i.e., $I = \langle I \rangle + \delta I$, $S_p = \langle S_p \rangle_m + \delta S_p$, $R_p = \langle R_p \rangle_m + \delta R_p$, and $P_h = \langle P_h \rangle + \delta P_h$, we have

$$\frac{d}{dt} \begin{pmatrix} \delta I \\ \delta S_p \\ \delta R_p \\ \delta P_h \end{pmatrix} = \begin{pmatrix} -J_{II} & J_{IS_p} & J_{IR_p} & J_{IP_h} \\ J_{S_pI} & -J_{S_pS_p} & J_{S_pR_p} & J_{S_pP_h} \\ J_{R_pI} & J_{R_pS_p} & -J_{R_pR_p} & -J_{R_pP_h} \\ J_{P_hI} & J_{P_hS_p} & J_{P_hR_p} & -J_{P_hP_h} \end{pmatrix} \times \begin{pmatrix} \delta I \\ \delta S_p \\ \delta R_p \\ \delta P_h \end{pmatrix} + \begin{pmatrix} \xi_I \\ \xi_{S_p} \\ \xi_{R_p} \\ \xi_{P_h} \end{pmatrix}, \tag{6}$$

with

$$\begin{aligned} J_{II} &= k_{dI}, \quad J_{IS_p} = J_{IR_p} = J_{IP_h} = 0, \\ J_{S_pI} &= k_p[S_T - \langle S_p \rangle_m], \\ J_{S_pS_p} &= k_p \langle I \rangle + k_{dp} + k_k[R_T - \langle R_p \rangle_m], \\ J_{S_pR_p} &= k_k \langle S_p \rangle_m, \quad J_{S_pP_h} = J_{R_pI} = 0, \\ J_{R_pS_p} &= k_k[R_T - \langle R_p \rangle_m], \\ J_{R_pR_p} &= k_k \langle S_p \rangle_m + k_{pm} \langle P_h \rangle, \quad J_{R_pP_h} = k_{pm} \langle R_p \rangle_m, \\ J_{P_hI} &= J_{P_hS_p} = J_{P_hR_p} = 0. \end{aligned}$$

Fourier transformation $[\delta \tilde{X}(\omega) = \int_{-\infty}^{+\infty} \delta X(t) \exp(-i\omega t)\, dt]$ of Eq. (6) gives

$$\begin{pmatrix} i\omega\delta\tilde{I} \\ i\omega\delta\tilde{S}_p \\ i\omega\delta\tilde{R}_p \\ i\omega\delta\tilde{P}_h \end{pmatrix} = \begin{pmatrix} -J_{II} & J_{IS_p} & J_{IR_p} & J_{IP_h} \\ J_{S_pI} & -J_{S_pS_p} & J_{S_pR_p} & J_{S_pP_h} \\ J_{R_pI} & J_{R_pS_p} & -J_{R_pR_p} & -J_{R_pP_h} \\ J_{P_hI} & J_{P_hS_p} & J_{P_hR_p} & -J_{P_hP_h} \end{pmatrix} \times \begin{pmatrix} \delta\tilde{I} \\ \delta\tilde{S}_p \\ \delta\tilde{R}_p \\ \delta\tilde{P}_h \end{pmatrix} + \begin{pmatrix} \tilde{\xi}_I \\ \tilde{\xi}_{S_p} \\ \tilde{\xi}_{R_p} \\ \tilde{\xi}_{P_h} \end{pmatrix}. \tag{7}$$

Solving Eq. (7) yields

$$\begin{aligned} (i\omega + J_{S_pS_p})\delta\tilde{S}_p &= J_{S_pI}\delta\tilde{I} + J_{S_pR_p}\delta\tilde{R}_p + \tilde{\xi}_{S_p}, \\ (i\omega + J_{R_pR_p})\delta\tilde{R}_p &= J_{R_pS_p}\delta\tilde{S}_p - J_{R_pP_h}\delta\tilde{P}_h + \tilde{\xi}_{R_p}, \\ (i\omega + J_{II})\delta\tilde{I} &= \tilde{\xi}_I, \quad (i\omega + J_{P_hP_h})\delta\tilde{P}_h = \tilde{\xi}_{P_h}, \end{aligned}$$

which finally leads to the desired expression of $\delta\tilde{R}_p$ for the monofunctional system,

$$\begin{aligned} \delta\tilde{R}_p = {} & \frac{J_{R_pS_p}J_{S_pI}\delta\tilde{I}}{(i\omega + J_{R_pR_p})(i\omega + J_{S_pS_p}) - J_{R_pS_p}J_{S_pR_p}} \\ & - \frac{[(i\omega + J_{S_pS_p})J_{R_pP_h}]\delta\tilde{P}_h}{(i\omega + J_{R_pR_p})(i\omega + J_{S_pS_p}) - J_{R_pS_p}J_{S_pR_p}} \\ & + \frac{(i\omega + J_{S_pS_p})\tilde{\xi}_{R_p}}{(i\omega + J_{R_pR_p})(i\omega + J_{S_pS_p}) - J_{R_pS_p}J_{S_pR_p}} \\ & + \frac{J_{R_pS_p}\tilde{\xi}_{S_p}}{(i\omega + J_{R_pR_p})(i\omega + J_{S_pS_p}) - J_{R_pS_p}J_{S_pR_p}}, \end{aligned} \tag{8}$$

where

$$\delta\tilde{I} = \frac{\tilde{\xi}_I}{i\omega + J_{II}}, \quad \delta\tilde{P}_h = \frac{\tilde{\xi}_{P_h}}{i\omega + J_{P_hP_h}}. \tag{9}$$

In Eq. (8), the first term arises due to external inducer I. The second term is due to fluctuations in the phosphatase activity of P_h on R_p. The third and fourth terms arise due to fluctuations in R_p and S_p, respectively. Now, using the expression of $\delta\tilde{R}_p$ given in Eq. (8) and employing the properties of the linear noise approximation given in Eqs. (5a)–(5d), we define the variance associated with R_p for the monofunctional system,

$$\begin{aligned}\sigma^2_{R_p} &= \frac{1}{2\pi}\int d\omega\langle|\delta\tilde{R}_p(\omega)|^2\rangle_m,\\ &= \frac{J^2_{R_pS_p}J^2_{S_pI}\langle I\rangle(\alpha_m+\beta_m+J_{II})}{\alpha_m\beta_m(\alpha_m+\beta_m)(\alpha_m+J_{II})(\beta_m+J_{II})} + \frac{J^2_{R_pP_h}\langle P_h\rangle}{\alpha_m\beta_m}\\ &\times\frac{\left(\beta_m+J_{P_hP_h}\right)J^2_{S_pS_p}+\alpha_m\left(\beta_m J_{P_hP_h}+J^2_{S_pS_p}\right)}{(\alpha_m+\beta_m)\left(\alpha_m+J_{P_hP_h}\right)\left(\beta_m+J_{P_hP_h}\right)}\\ &+\frac{\gamma_m+k_k\langle S_p\rangle_m[R_T-\langle R_p\rangle_m]\left(J^2_{S_pS_p}+\alpha_m\beta_m\right)}{\alpha_m\beta_m(\alpha_m+\beta_m)},\end{aligned} \tag{10}$$

with

$$\begin{aligned}\alpha_m &= \tfrac{1}{2}\big[\left(J_{S_pS_p}+J_{R_pR_p}\right)\\ &\quad+\left\{\left(J_{S_pS_p}-J_{R_pR_p}\right)^2+4J_{S_pR_p}J_{R_pS_p}\right\}^{1/2}\big],\\ \beta_m &= \tfrac{1}{2}\big[\left(J_{S_pS_p}+J_{R_pR_p}\right)\\ &\quad-\left\{\left(J_{S_pS_p}-J_{R_pR_p}\right)^2+4J_{S_pR_p}J_{R_pS_p}\right\}^{1/2}\big],\\ \gamma_m &= J^2_{R_pS_p}k_p(S_T-\langle S_p\rangle_m)\langle I\rangle\\ &\quad-J_{R_pS_p}J_{S_pS_p}k_k\langle S_p\rangle_m(R_T-\langle R_p\rangle_m).\end{aligned}$$

B. Bifunctional system

Considering the kinetic steps given by Eqs. (1b), (1c), and (1f) and fluctuations associated with them, the Langevin equations for S_p and R_p for the bifunctional system can be written as follows:

$$\frac{dS_p}{dt} = k_p(S_T-S_p)I - k_{dp}S_p - k_kS_p(R_T-R_p) + \xi_{S_p}, \tag{11a}$$

$$\frac{dR_p}{dt} = k_kS_p(R_T-R_p) - k_{pb}R_p(S_T-S_p) + \xi_{R_p}. \tag{11b}$$

The additive noise terms ξ_{S_p} and ξ_{R_p} take care of fluctuations in the copy number of S_p and R_p, respectively. The statistical properties of the two fluctuating terms are given by [33–35]

$$\langle\xi_{S_p}(t)\xi_{S_p}(t+\tau)\rangle_b = 2k_p[S_T-\langle S_p\rangle_b]\langle I\rangle\delta(\tau), \tag{12a}$$

$$\langle\xi_{R_p}(t)\xi_{R_p}(t+\tau)\rangle_b = 2k_k\langle S_p\rangle_b[R_T-\langle R_p\rangle_b]\delta(\tau), \tag{12b}$$

with $\langle\xi_{S_p}(t)\rangle_b = \langle\xi_{R_p}(t)\rangle_b = 0$. In the above equations, $\langle S_p\rangle_b$ and $\langle R_p\rangle_b$ stand for the mean values of S_p and R_p at the steady state, respectively. Here $\langle\cdots\rangle_b$ has been used to designate the ensemble average for a bifunctional system. As in a monofunctional system, we consider the noise terms ξ_{S_p} and ξ_{R_p} to be correlated [30,36],

$$\langle\xi_{S_p}(t)\xi_{R_p}(t+\tau)\rangle_b = -k_k\langle S_p\rangle_b[R_T-\langle R_p\rangle_b]\delta(\tau). \tag{12c}$$

At this point it is important to note the difference between Eq. (4b) and Eq. (11b). In Eq. (4b), the loss term ($k_{pm}P_hR_p$) appears due to phosphatase activity of P_h on R_p, whereas in Eq. (11b), the loss term ($k_{pb}R_p(S_T-S_p)$) appears due to phosphatase activity of S on R_p. Although the noise term ξ_{R_p} in both Eqs. (4b) and (11b) looks almost the same, it is the loss term in the aforesaid equations that makes the steady-state behavior of R_p different in monofunctional and bifunctional systems. Now, linearizing as usual around the mean value at steady state, we have

$$\begin{aligned}\frac{d}{dt}\begin{pmatrix}\delta I\\ \delta S_p\\ \delta R_p\end{pmatrix} &= \begin{pmatrix}-J_{II} & J_{IS_p} & J_{IR_p}\\ J_{S_pI} & -J_{S_pS_p} & J_{S_pR_p}\\ J_{R_pI} & J_{R_pS_p} & -J_{R_pR_p}\end{pmatrix}\\ &\times\begin{pmatrix}\delta I\\ \delta S_p\\ \delta R_p\end{pmatrix}+\begin{pmatrix}\xi_I\\ \xi_{S_p}\\ \xi_{R_p}\end{pmatrix},\end{aligned} \tag{13}$$

with

$$\begin{aligned}&J_{II} = k_{dI}, \quad J_{IS_p} = J_{IR_p} = 0, \quad J_{SpI} = k_p[S_T-\langle S_p\rangle_b],\\ &J_{S_pS_p} = k_p\langle I\rangle + k_{dp} + k_k[R_T-\langle R_p\rangle_b], \quad J_{S_pR_p} = k_k\langle S_p\rangle_b,\\ &J_{R_pI} = 0, \quad J_{R_pS_p} = k_k[R_T-\langle R_p\rangle_b] + k_{pb}\langle R_p\rangle_b,\\ &J_{R_pR_p} = k_k\langle S_p\rangle_b + k_{pb}[S_T-\langle S_P\rangle_b].\end{aligned}$$

Fourier transforming Eq. (13) yields

$$\begin{aligned}\begin{pmatrix}i\omega\delta\tilde{I}\\ i\omega\delta\tilde{S}_p\\ i\omega\delta\tilde{R}_p\end{pmatrix} &= \begin{pmatrix}-J_{II} & J_{IS_p} & J_{IR_p}\\ J_{S_pI} & -J_{S_pS_p} & J_{S_pR_p}\\ J_{R_pI} & J_{R_pS_p} & -J_{R_pR_p}\end{pmatrix}\\ &\times\begin{pmatrix}\delta\tilde{I}\\ \delta\tilde{S}_p\\ \delta\tilde{R}_p\end{pmatrix}+\begin{pmatrix}\tilde{\xi}_I\\ \tilde{\xi}_{S_p}\\ \tilde{\xi}_{R_p}\end{pmatrix},\end{aligned} \tag{14}$$

the solution of which eventually leads to

$$\begin{aligned}\left(i\omega+J_{S_pS_p}\right)\delta\tilde{S}_p &= J_{S_pI}\delta\tilde{I} + J_{S_pR_p}\delta\tilde{R}_p + \tilde{\xi}_{S_p}\\ \left(i\omega+J_{R_pR_p}\right)\delta\tilde{R}_p &= J_{R_pS_p}\delta\tilde{S}_p + \tilde{\xi}_{R_p}.\end{aligned}$$

Using the above two relations, we have the desired expression of $\delta\tilde{R}_p$ for the bifunctional system,

$$\begin{aligned}\delta\tilde{R}_p &= \frac{J_{R_pS_p}J_{S_pI}\delta\tilde{I}}{\left(i\omega+J_{R_pR_p}\right)\left(i\omega+J_{S_pS_p}\right)-J_{R_pS_p}J_{S_pR_p}}\\ &+\frac{\left(i\omega+J_{S_pS_p}\right)\tilde{\xi}_{R_p}}{\left(i\omega+J_{R_pR_p}\right)\left(i\omega+J_{S_pS_p}\right)-J_{R_pS_p}J_{S_pR_p}}\\ &+\frac{J_{R_pS_p}\tilde{\xi}_{S_p}}{\left(i\omega+J_{R_pR_p}\right)\left(i\omega+J_{S_pS_p}\right)-J_{R_pS_p}J_{S_pR_p}},\end{aligned} \tag{15}$$

where the expression for $\delta\tilde{I}$ is given in Eq. (9). Now, using the expression for $\delta\tilde{R}_p$ and properties of the linear noise expression given in Eqs. (12a)–(12c), we write the variance associated

with R_p for the bifunctional system,

$$\sigma^2_{R_p} = \frac{1}{2\pi}\int d\omega \langle|\delta\tilde{R}_p(\omega)|^2\rangle_b,$$
$$= \frac{J^2_{R_pS_p}J^2_{S_pI}\langle I\rangle(\alpha_b+\beta_b+J_{II})}{\alpha_b\beta_b(\alpha_b+\beta_b)(\alpha_b+J_{II})(\beta_b+J_{II})}$$
$$+\frac{\gamma_b + k_k\langle S_p\rangle_b[R_T-\langle R_p\rangle_b]\left(J^2_{S_pS_p}+\alpha_b\beta_b\right)}{\alpha_b\beta_b(\alpha_b+\beta_b)}, \quad (16)$$

with

$$\alpha_b = \tfrac{1}{2}\Big[\left(J_{S_pS_p}+J_{R_pR_p}\right) + \left\{\left(J_{S_pS_p}-J_{R_pR_p}\right)^2 + 4J_{S_pR_p}J_{R_pS_p}\right\}^{1/2}\Big],$$
$$\beta_b = \tfrac{1}{2}\Big[\left(J_{S_pS_p}+J_{R_pR_p}\right) - \left\{\left(J_{S_pS_p}-J_{R_pR_p}\right)^2 + 4J_{S_pR_p}J_{R_pS_p}\right\}^{1/2}\Big],$$
$$\gamma_b = J^2_{R_pS_p}k_p(S_T-\langle S_p\rangle_b)\langle I\rangle - J_{R_pS_p}J_{S_pS_p}k_k\langle S_p\rangle_b(R_T-\langle R_p\rangle_b).$$

III. RESULTS AND DISCUSSION

Since the main objective of the TCS signal transduction motif is to transduce the external stimulus effectively and to generate the pool of phosphorylated response regulator R_p that regulates several downstream genes, we now focus on quantifying different physical quantities associated with R_p for monofunctional and bifunctional systems. While doing this, we make use of the expressions for R_p given by Eq. (10) and Eq. (16). Before proceeding further, it is important to mention the activity of kinase and phosphatase in monofunctional and bifunctional systems. In the monofunctional system, it has been observed that phosphatase has a higher affinity for the phosphorylated response regulator. On the other hand, in the bifunctional system, unphosphorylated sensor kinase has a lower affinity for the same [6]. Following this experimental information, kinase and phosphatase rate constants for both systems could be $k_k/k_{pm} < k_k/k_{pb}$. However, following earlier work on the deterministic system, we consider $k_k/k_{pm} = k_k/k_{pb}$ as the particular parameter set as it has been shown to have a high degree of robustness [23]. Furthermore, to check the validity of our proposed model, we perform a stochastic simulation using the Gillespie algorithm [37,38] and find that the theoretical and numerical results are in good agreement with each other.

In Fig. 2(a), we show the mean R_p level at steady state, $\langle R_p\rangle$, as a function of the mean extracellular inducer level, $\langle I\rangle$. Initially, for a low inducer level, both profiles grow linearly. However, as the inducer level increases, the profile of $\langle R_p\rangle$ for the monofunctional system (solid line) grows hyperbolically, whereas the same for the bifunctional system grows linearly (dashed line). It is important to mention that linear growth is a signature of a linear input-output relation where the output level is dependent only on the input stimulus, which increases the autophosphorylation rate in the model [12]. The linear input-output relation for the bifunctional system can be derived easily from Eq. (11), which provides the expression for mean

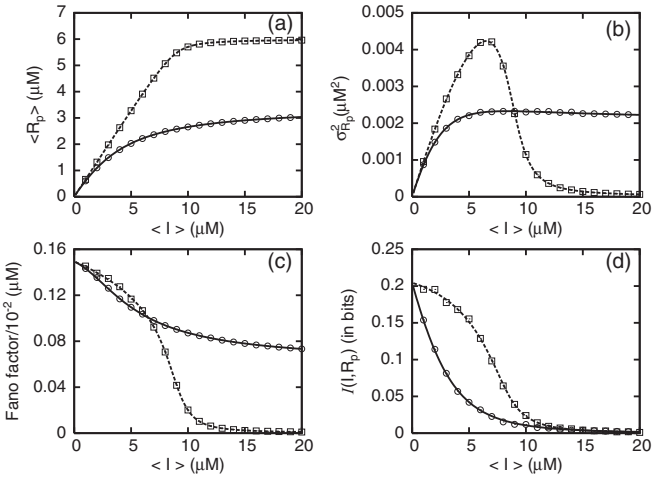

FIG. 2. Steady-state (a) $\langle R_p\rangle$ level, (b) $\sigma^2_{R_p}$, (c) the Fano factor $(\sigma^2_{R_p}/\langle R_p\rangle)$, and (d) mutual information $\mathcal{I}(I,R_p)$ as a function of mean extracellular inducer level. In all panels, solid (with open circles) and dashed (with open squares) lines are for the monofunctional and bifunctional systems, respectively. The symbols are generated using the stochastic simulation algorithm [37,38] and the lines are due to theoretical calculation. The parameters used are [23] $k_p = 0.1\ \mu\text{M}^{-1}\ \text{s}^{-1}$, $k_{dp} = 0.01\ \text{s}^{-1}$, $k_k = 0.2\ \mu\text{M}^{-1}\ \text{s}^{-1}$, $k_{pb} = 0.15\ \mu\text{M}^{-1}\ \text{s}^{-1}$, $k_{pm} = 0.15\ \mu\text{M}^{-1}\ \text{s}^{-1}$, $k_{sP_h} = 0.3\ \mu\text{M}\ \text{s}^{-1}$, $k_{dP_h} = 0.1\ \text{s}^{-1}$, $S_T = 3.0\ \mu\text{M}$, and $R_T = 6.0\ \mu\text{M}$.

R_p level at steady state [24],

$$\langle R_p\rangle = \frac{1}{2}\left(R_T + \frac{k_{dp}}{k_k} + \frac{k_p\langle I\rangle}{k_{pb}}\right) - \frac{1}{2}\sqrt{\left(R_T + \frac{k_{dp}}{k_k} + \frac{k_p\langle I\rangle}{k_{pb}}\right)^2 - \frac{4k_p\langle I\rangle R_T}{k_{pb}}}.$$

For $R_T > (k_{dp}/k_k) + (k_p\langle I\rangle/k_{pb})$, we have $\langle R_p\rangle \approx (k_p/k_{pb})\langle I\rangle$, showing a linear relation between the input signal and the output. On the other hand, using Eq. (4), one can derive the mean R_p level at steady state for a monofunctional system which takes into account both signals (input stimulus and phosphatase) as well as the steady-state value of the mean S_p,

$$\langle R_p\rangle = \frac{k_p\langle I\rangle S_T - (k_p\langle I\rangle + k_{dp})\langle S_p\rangle}{k_{pm}\langle P_h\rangle}.$$

In this connection, it is important to mention that TetR-based negative autoregulation has been reported to linearize the dose-response (input-output) relation in *Saccharomyces cerevisiae* [39].

Figure 2(a) further shows that for a fixed stimulus, the amount of R_p is always higher for the bifunctional TCS. Thus, for a fixed stimulus, the phosphotransfer mechanism is more effective in producing a pool of R_p for the bifunctional system compared to the monofunctional one and is in agreement with the result proposed earlier [21]. Biologically, generation of a larger pool of R_p is quite significant when it comes to the phenomenon of gene regulation, as R_p acts as a transcription factor for several downstream genes. In the mechanism of gene regulation, a specific transcription factor needs to attain a threshold value to make the genetic switch operative. Our result

suggests that for a target gene, a bifunctional system might work more effectively than a monofunctional one by attaining the required pool of R_p earlier. Due to such a high activity, the bifunctional system will respond to a certain stimulus earlier than the monofunctional system by regulating downstream genes.

Figure 2(b) shows the profile of $\sigma^2_{R_p}$ and the variance of R_p. For the monofunctional system, the variance grows steadily and then remains almost constant (solid line). However, the variance profile of the bifunctional system first grows to a maximum and then starts going down (dashed line). At a critical value of the extracellular inducer level, almost all sensors and response regulators in the bifunctional system become phosphorylated, which, in turn, decrease fluctuations associated with R_p. Lowering of fluctuations in R_p thereby reduces the variance. For the monofunctional case, in addition to the phosphorylation by the sensor kinase, an additional strong phosphatase activity is operational in the system which maintains sufficient fluctuations in the R_p level, henceforth keeping the variance constant.

In the calculation of the variance for the monofunctional system [see Eq. (10)], we have considered two extra sources of fluctuations, one due to the fluctuations in the kinetics of the extracellular signal [Eq. (1a)] and the other due to the fluctuations in the kinetics of phosphatase P_h [Eq. (1e)]. It is thus interesting to analyze whether fluctuations due to P_h do have any significant role in the variance of the monofunctional system. In the expression of $\delta\tilde{R}_p$ for the monofunctional system [see Eq. (8)], the second term appears due to the stochastic kinetics associated with the phosphatase P_h [see Eq. (4c)]. However, for a constant level of phosphatase, i.e., $\langle P_h\rangle$, one does not need to consider the stochastic kinetics given by Eq. (4c) that effectively removes fluctuations associated with P_h from both Eq. (8) and Eq. (10). In addition, the mean-field contribution of P_h appears in the second term on the right-hand side of Eq. (4b). Thus, for $\langle P_h\rangle$, the expression of the variance for the monofunctional system becomes

$$\sigma^2_{R_p} = \frac{J^2_{R_pS_p} J^2_{S_pI}\langle I\rangle(\alpha_m+\beta_m+J_{II})}{\alpha_m\beta_m(\alpha_m+\beta_m)(\alpha_m+J_{II})(\beta_m+J_{II})} + \frac{\gamma_m + k_k\langle S_p\rangle_m[R_T-\langle R_p\rangle_m]\left(J^2_{S_pS_p}+\alpha_m\beta_m\right)}{\alpha_m\beta_m(\alpha_m+\beta_m)}. \quad (17)$$

In Fig. 3, we show the variance associated with R_p for the monofunctional system. The solid and dotted lines are due to the presence and absence of fluctuations in P_h, respectively. It is clear from the profiles that for a constant level of phosphatase, $\sigma^2_{R_p}$ reduces appreciably compared to the fluctuating P_h level. This result suggests that stochastic kinetics of P_h has a significant role in the fluctuations associated with R_p in the monofunctional system.

To quantify cellular fluctuations that affect the phospho-transfer mechanism within the TCS, we calculate the Fano factor ($\sigma^2_{R_p}/\langle R_p\rangle$) [34,40] at steady state. In Fig. 2(c), we have shown the profile of the Fano factor for the monofunctional and the bifunctional systems (solid and dashed lines, respectively) as a function of the mean extracellular inducer level, where both profiles show decaying characteristics. Beyond a certain inducer level, the Fano factor for the bifunctional system

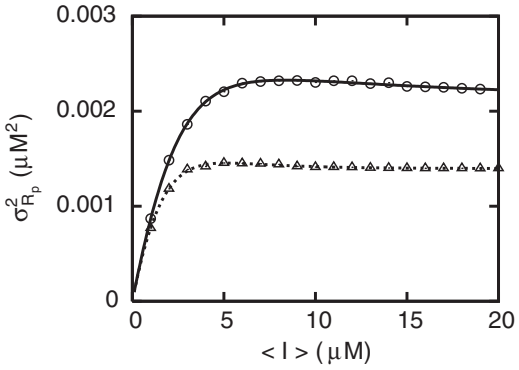

FIG. 3. Steady-state variance $\sigma^2_{R_p}$ of the monofunctional system. The solid (with open circle) and dotted (with open triangle) lines are due to fluctuating P_h and constant P_h ($\langle P_h\rangle$), respectively. The symbols are generated using stochastic simulation algorithm [37,38] and the lines are due to theoretical calculation. For constant P_h, we have used $\langle P_h\rangle = 3\ \mu$M. The parameters used are same as in Fig. 2.

(dashed line) abruptly goes down to zero, which can be attributed to the decaying nature of its variance, shown in Fig. 2(b). The pool of R_p generated in the monofunctional system is not high enough to overcome fluctuations induced by the phosphatase P_h and, as a result, the fluctuations for this system maintain a low nonzero value compared to the bifunctional system. In addition to the Fano factor, we have also calculated the coefficient of variation (CV), i.e., $\sigma_{R_p}/\langle R_p\rangle$. In Fig. 4, we show the steady-state CV profile for both monofunctional and bifunctional systems.

As mentioned earlier, the specific job of a TCS is to sense change in the extracellular environment and to transduce this information downstream reliably. To check how functionality of the sensor kinase affects fidelity (signal-to-noise ratio) of the signal processing mechanism, we calculate the quantity mutual information $\mathcal{I}(I,R_p)$ using the definition of Shannon [41,42],

$$\mathcal{I}(I,R_p) = \frac{1}{2}\log_2\left(1+\frac{\sigma^4_{IR_p}}{|C|}\right); \quad C = \begin{pmatrix}\sigma^2_{II} & \sigma^2_{IR_p}\\ \sigma^2_{IR_p} & \sigma^2_{R_pR_p}\end{pmatrix},$$

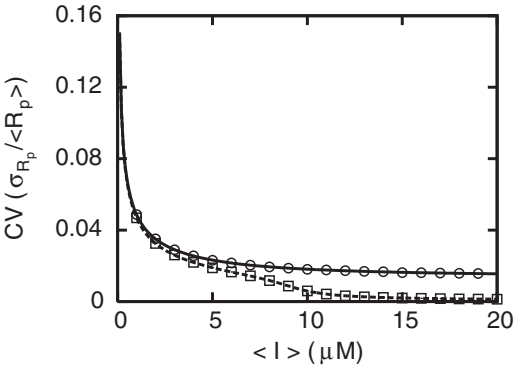

FIG. 4. Steady-state CV ($\sigma_{R_p}/\langle R_p\rangle$) as a function of mean extracellular inducer level. The solid (with open circles) and dashed (with open squares) lines are for the monofunctional and bifunctional systems, respectively. The symbols are generated using a stochastic simulation algorithm [37,38] and the lines are due to theoretical calculation. The parameters used are same as in Fig. 2.

where

$$\sigma_{II}^2 = \langle I \rangle, \quad \sigma_{IR_p}^2 = \frac{J_{R_p S_p} J_{S_p I} \langle I \rangle}{(\alpha_i + J_{II})(\beta_i + J_{II})}.$$

In the above relation, $i = m$ or $i = b$ depending on the monofunctional and bifunctional systems, respectively. Expressions for $\sigma_{R_p R_p}^2 (\equiv \sigma_{R_p}^2)$ are given in Eqs. (10) and (16) for the two systems, respectively. Note that the quantity $\sigma_{IR_p}^4 / |C|$ stands for the fidelity or signal-to-noise ratio [43,44].

In Fig. 2(d), we show the mutual information profile for the monofunctional (solid line) and the bifunctional (dashed line) systems as a function of the extracellular inducer level. Information processing by both systems show a decaying profile as the extracellular inducer level is increased. However, for a wide range of inducer level, information processing by the bifunctional system is higher than the monofunctional one. Beyond a certain value of the inducer level, the information profile of the bifunctional system goes down and becomes equal to the profile of the monofunctional system. This result suggests that reliability of the bifunctional system in processing the information of the extracellular environment is higher than that of the monofunctional system.

To check the specific role of the kinase and phosphatase rates on information processing within the TCS further, we calculate the Fano factor and $\mathcal{I}(I, R_p)$ as a function of the kinase and phosphatase rates. In Figs. 5(a)–5(b), we show a two-dimensional map of the Fano factor and mutual information, respectively, for the monofunctional system as a function of k_k and k_{pm}. Figures 5(c)–5(d) show the same for the bifunctional system as a function of k_k and k_{pb}. Figure 5(a) shows that for high kinase and moderate phosphatase rates, the fluctuations level of phosphorylated response regulator becomes maximum, otherwise it maintains a low value. This happens due to low copy number of proteins produced under the high-phosphatase regime. For the bifunctional system, the fluctuations level maintains a low value for a wide range of kinase and low phosphatase rates [see Fig. 5(c)]. Other than that, the fluctuations increase due to the increase in the phosphatase activity of the sensor protein. It is important to mention that the maximum fluctuation level for the bifunctional system spans a wider region in the kinase-phosphatase plane compared to the monofunctional system. Figures 5(b) and 5(d) show mutual information for the monofunctional and bifunctional systems, respectively. In both cases, signal processing capacity increases for the high kinase and high phosphatase rates. In the regime of high kinase and high phosphatase activity, fluctuations in the R_p copy number can reliably sense the fluctuations due to the extracellular stimulus which, in turn, effectively increases the signal processing capacity. In addition, due to structural advantage, information processing is better for the bifunctional system.

Our analysis suggests that the bifunctional system can transduce external stimulus more reliably than the monofunctional one. The effective signal transduction mechanism of the bifunctional system can be attributed to its sensor domain, which has synchronized kinase and phosphatase activity. On the other hand, the monofunctional system lacks such a synchronization due to the absence of phosphatase activity in the sensor domain. At this point, one can ask the question, "Is it possible to increase the activity of a monofunctional system by varying the contribution of one or more system components?" To answer this question we further looked

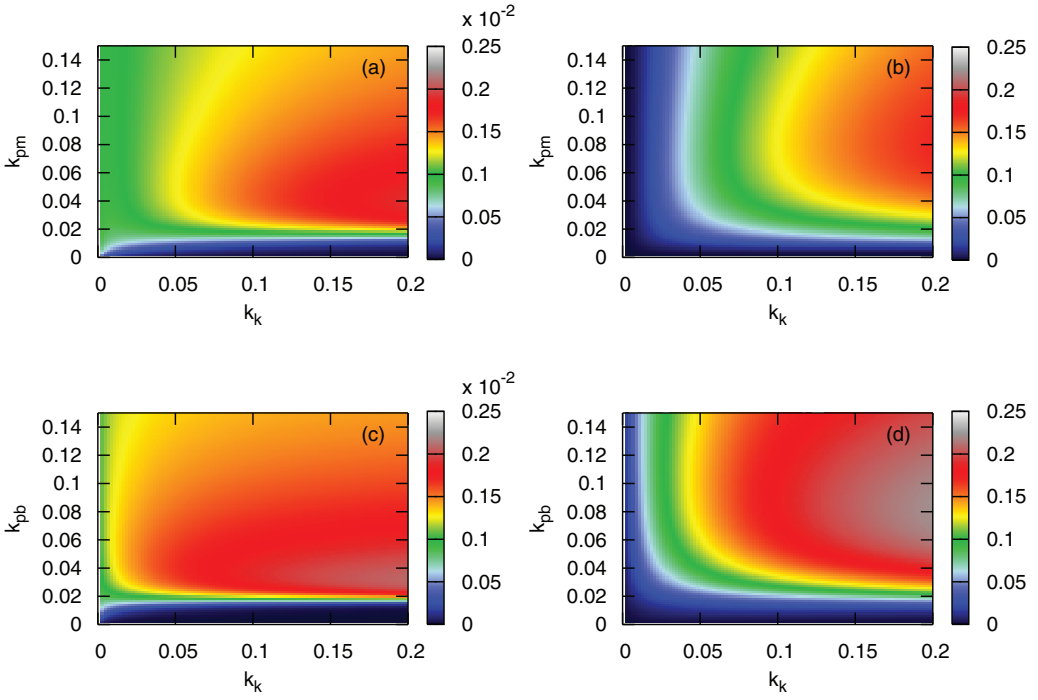

FIG. 5. (Color online) Two-dimensional map of the Fano factor and mutual information, repectively, for the monofunctional [(a) and (b)] and bifunctional systems [(c) and (d)] as a function of the kinase and phosphatase rates. The two-dimensional map is a projection of the Fano factor and mutual information on the kinase and phosphatase planes. All panels are drawn using $\langle I \rangle = 1$ μM. Values of other parameters are the same as in Fig. 2.

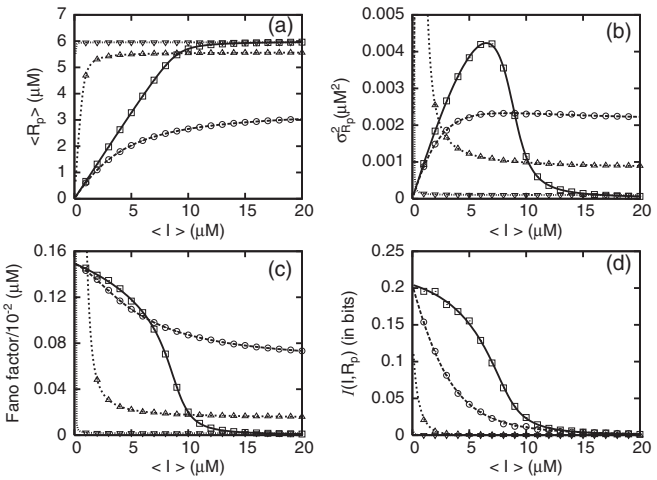

FIG. 6. The role of P_h in (a) $\langle R_p \rangle$, (b) $\sigma^2_{R_p}$, (c) the Fano factor, and (d) $\mathcal{I}(I, R_p)$ for the monofunctional system. The open circle, up-triangle, and down-triangle stand for $P_h = 3.0$, 0.3, and 0.03, respectively (all in μM). Profile of bifunctional system (solid line with squares) has been shown in all four panels for reference. Values of the other parameters are same as in Fig. 2.

into the signal transduction motif of the monofunctional system and found that, due to the auxiliary protein P_h, the monofunctional TCS is unable to attain the activity of the bifunctional one. Using this phenomenological information, one may hypothesize that by reducing the effect of P_h, activity of the monofunctional system can be increased. To check this hypothesis, we have systematically reduced the concentration of P_h by reducing the synthesis rate (k_{sP_h}) of P_h from a high to a low value and calculated all physical quantities reported in Fig. 2 (see Fig. 6). As the level of P_h goes down, the phosphatase activity on the response regulator becomes more ineffective and, hence, increases the pool of R_p [see Fig. 6(a)]. For a low amount of P_h, R_p level reaches the maximum value, as attained by the bifunctional system, quite early. This suggests that using the parameter set of the model and by lowering the amount of P_h, a monofunctional system can attain a large pool of R_p even at a very low level of inducer. At a very low level of P_h, most of the response regulators get phosphorylated, henceforth reducing fluctuations in the R_p level [see Figs. 6(b) and 6(c)]. Interestingly, mutual information for the monofunctional system goes down with the lowering of P_h [see Fig. 6(d)]. By reducing the level of P_h, fluctuations in the R_p level can be reduced, which, in turn, makes the system independent of fluctuations due to an external stimulus. As a result, one observes suppression of mutual information.

Fluctuations due to inherent noisy biochemical reactions play an important role in gene regulation by imposing phenotypic heterogeneity within genetically identical cells [7,16]. This happens due to fluctuation-induced distributions of proteins in identical cells. In the present study, the TCS network output (R_p) shows the maximal and minimal levels of fluctuations for low and high stimuli, respectively. In addition, the bifunctional system maintains a lower noise profile compared to the monofunctional one. These results together suggest that the bifunctional-system-controlled gene regulation may have lower variability (a lower Fano factor) compared to the monofunctional system for intermediate to high stimulus levels. To verify the difference in variability in TCS-controlled gene regulation, we consider a simple model of gene expression in the following section.

A. TCS-mediated gene regulation

To understand the role of TCS on downstream genes, we consider a simple model of gene regulation mediated by either monofunctional or bifunctional TCSs,

$$\xrightarrow{k_1 f(R_p)} X \xrightarrow{k_2} \varnothing, \tag{18}$$

where X is the gene product whose synthesis is controlled by the transcription factor R_p, the output of the TCS. The function $f(R_p)$ takes care of the promoter switching mechanism associated with the downstream gene and is given by $f(R_p) = R_p/(K + R_p)$, with K being the binding constant. While modeling the promoter switching mechanism, we have considered positive regulation by R_p. The stochastic differential equation associated with Eq. (18) is given by

$$\frac{dX}{dt} = k_1 f(R_p) - k_2 X + \xi_X, \tag{19}$$

with $\langle \xi_X(t) \rangle = 0$ and $\langle \xi_X(t) \xi_X(t') \rangle = 2k_2 \langle X \rangle \delta(t - t')$. A Fourier transformation of the linearized version of Eq. (19) yields

$$\delta \tilde{X}(\omega) = k_1 \left[\frac{\delta f(R_p)}{\delta R_p} \right]_{\rm ss} \frac{\delta \tilde{R}_p(\omega)}{(i\omega + k_2)} + \frac{\tilde{\xi}_X(\omega)}{(i\omega + k_2)}, \tag{20}$$

where $[\delta f(R_p)/\delta R_p]_{\rm ss} = K/(K + \langle R_p \rangle)^2$, evaluated at steady state (ss). Now, using the expression $\delta \tilde{X}$, we derive the variance associated with X,

$$\sigma^2_X = k_1^2 \left[\frac{\delta f(R_p)}{\delta R_p} \right]^2_{\rm ss} \frac{\sigma^2_{R_p}}{k_2} + \langle X \rangle. \tag{21}$$

Note that in Eq. (21), fluctuations due to the output of the TCS is embedded in the expression of $\sigma^2_{R_p}$, which differs for the monofunctional and the bifunctional systems [see Eq. (10) and Eq. (16), respectively].

The main panel of Fig. 7 shows the steady state $\langle X \rangle$ as a function of the mean inducer level $\langle I \rangle$ controlled by the monofunctional (solid line with open circle) and bifunctional systems (dashed line with open square). It is evident from the profiles of $\langle X \rangle$ that the bifunctional-regulated system produces more downstream protein as $\langle I \rangle$ is increased. This happens due to the availability of larger amounts of $\langle R_p \rangle$ produced by the bifunctional system compared to the monofunctional one for a fixed amount of $\langle I \rangle$ [see Fig. 2(a)]. Figure 7(b) depicts the Fano factor ($\sigma^2_X/\langle X \rangle$) associated with the downstream protein and shows that fluctuations in X controlled by the bifunctional system are lower compared to those of the monofunctional system. Fluctuations in X are controlled by fluctuations in R_p, as shown in Eq. (21). As fluctuations associated with R_p due to the bifunctional system are lower than those in the monofunctional system [see Fig. 2(c)], its contribution in the Fano factor associated with X is low.

In the previous discussion, we have shown that for a fixed level of inducer, a bifunctional system produces more R_p

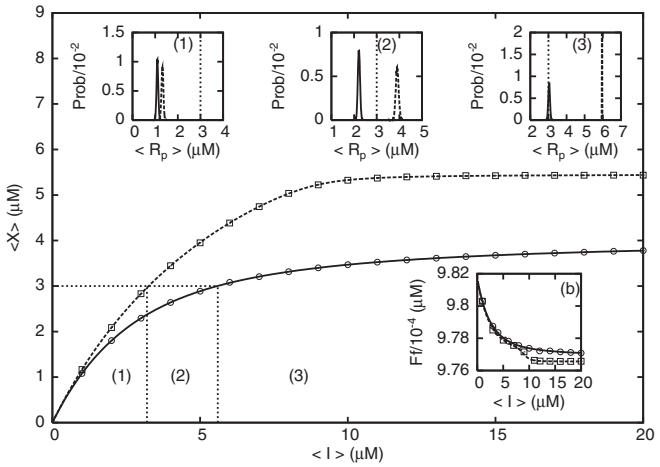

FIG. 7. Steady state $\langle X\rangle$ as a function of inducer $\langle I\rangle$. The solid (with open circle) and dashed (with open square) lines are the $\langle X\rangle$ profile generated by the monofunctional and bifunctional systems, respectively. Note that the lines and symbols are due to theory and simulation [37,38], respectively. The horizontal dotted line is for the target $\langle X\rangle$ value and the vertical dotted lines are the corresponding inducer levels for monofunctional and bifunctional systems. (1), (2), and (3) correspond to three different regions of $\langle I\rangle$ for a fixed target $\langle X\rangle$. Inset (b): The Fano factor (Ff) for X as a function of $\langle I\rangle$. Both lines and symbols are the same as in main figure. Insets (1)–(3): Probability distribution of R_p as a function of $\langle R_p\rangle$. The solid and dotted lines represent the probability distribution of R_p for the monofunctional and bifunctional systems, respectively. The vertical dotted line denotes the value of target $\langle X\rangle$ as shown in the main figure. The parameters used are $K = 5\ \mu$M, $k_1 = 3 \times 10^{-3}\ \mu\text{M s}^{-1}$, $k_2 = 3 \times 10^{-4}\ \text{s}^{-1}$ and the values of the other parameters are the same as in Fig. 2.

compared to a monofunctional system [see Fig. 2(a)]. From this observation, we commented that a bifunctional system is more effective than a monofunctional one in regulating downstream genes for intermediate to high inducer levels. To verify our remark, we numerically calculate the probability distribution of R_p (transcription factor for target gene) for monofunctional and bifunctional systems [solid and dashed lines in insets (1)–(3) of Fig. 7] for different values of $\langle I\rangle$ and check whether they are able to cross the fixed $\langle X\rangle$ value [vertical dotted line in insets (1)–(3) of Fig. 7]. The distribution profiles give an idea of whether the pool of R_p is able to generate a fixed level of gene product, in the presence of inducer. For this, we set the value of the downstream product X at 3 μM (horizontal dotted line in the main panel of Fig. 7), which intercepts both profiles of $\langle X\rangle$ at two different values of $\langle I\rangle$. To be explicit, for $\langle I\rangle = 3.2\,\mu$M and 5.6 μM, the horizontal dotted line intercepts the profile of the bifunctional and monofunctional systems, respectively. This, in turn, generates three different regions of $\langle I\rangle$ [(1), (2), and (3)], shown in the main panel of Fig. 7. When the value of $\langle I\rangle$ lies within region (1), the distribution profiles of R_p for both systems are unable to cross the required value of $\langle X\rangle$ [inset (1) of Fig. 7]. This scenario changes as we move to region (2). In this region, the distribution profile of the bifunctional system crosses the target $\langle X\rangle$ value, but the distribution profile of the monofunctional system is unable to cross the same [inset (2) of Fig. 7)]. This happens due to the low and high pools of R_p generated by the monofunctional and bifunctional systems, respectively. As we further move to region (3), we see that the distribution profiles of both systems are able to cross the target $\langle X\rangle$ value as both produce enough R_p to achieve the goal.

IV. CONCLUSION

To conclude, we have developed a stochastic model for the signal transduction mechanism in bacterial TCSs. The proposed model takes into account the difference in the functionality of the sensor kinase. This difference in functionality leads to a classification of the TCS, viz., monofunctional and bifunctional. Considering only the phosphotransfer mechanism within a TCS triggered by an external stimulus, we have derived a Langevin equation associated with the system components for both systems (monofunctional and bifunctional). Using the expression of phosphorylated response regulators, we have calculated different physically realizable quantities, viz., the variance, the Fano factor (variance/mean), and mutual information at steady state. Our analysis suggests that at low external stimulus, both systems reliably transduce information due to changes made in the extracellular environment. Moreover, due to the functional difference of the sensor kinase, it has been observed that the fidelity of the bifunctional system is higher than that of the monofunctional system. The functionality of a monofunctional system has been predicted to be increasable by reducing the amount of auxiliary protein (P_h), which can be tested experimentally. We further extend our analysis by studying TCS-mediated gene regulation, which shows that the bifunctional system is more effective in producing target gene product for intermediate to high inducer levels with lower variability.

ACKNOWLEDGMENTS

We thank Debi Banerjee for critical reading of the manuscript. A.K.M. and A.B. are thankful to UGC [UGC/776/JRF(Sc)] and CSIR [09/015(0375)/2009-EMR-I], respectively, for support through a research fellowship. S.K.B acknowledges support from the Bose Institute through Institutional Programme VI-Development of Systems Biology.

[1] H. H. McAdams and L. Shapiro, Science **269**, 650 (1995).
[2] J. J. Tyson, K. C. Chen, and B. Novak, Curr. Opin. Cell Biol. **15**, 221 (2003).
[3] U. Alon, Nat. Rev. Genet. **8**, 450 (2007).
[4] A. H. West and A. M. Stock, Trends Biochem. Sci. **26**, 369 (2001).
[5] M. T. Laub and M. Goulian, Annu. Rev. Genet. **41**, 121 (2007).
[6] L. J. Kenney, Curr. Opin. Microbiol. **13**, 168 (2010).
[7] A. Tiwari, G. Balázsi, M. L. Gennaro, and O. A. Igoshin, Phys. Biol. **7**, 036005 (2010).
[8] W. Hsing, F. D. Russo, K. K. Bernd, and T. J. Silhavy, J. Bacteriol. **180**, 4538 (1998).

[9] S. D. Goldberg, G. D. Clinthorne, M. Goulian, and W. F. DeGrado, Proc. Natl. Acad. Sci. USA **107**, 8141 (2010).
[10] Y. Hart, Y. E. Antebi, A. E. Mayo, N. Friedman, and U. Alon, Proc. Natl. Acad. Sci. USA **109**, 8346 (2012).
[11] Y. Hart and U. Alon, Mol. Cell **49**, 213 (2013).
[12] G. Shinar, R. Milo, M. R. Martínez, and U. Alon, Proc. Natl. Acad. Sci. USA **104**, 19931 (2007).
[13] J. Paulsson, Nature **427**, 415 (2004).
[14] N. Rosenfeld, J. W. Young, U. Alon, P. S. Swain, and M. B. Elowitz, Science **307**, 1962 (2005).
[15] A. Zaslaver, A. Bren, M. Ronen, S. Itzkovitz, I. Kikoin, S. Shavit, W. Liebermeister, M. G. Surette, and U. Alon, Nat. Methods **3**, 623 (2006).
[16] M. Kaern, T. C. Elston, W. J. Blake, and J. J. Collins, Nat. Rev. Genet. **6**, 451 (2005).
[17] R. Silva-Rocha and V. de Lorenzo, Annu. Rev. Microbiol. **64**, 257 (2010).
[18] A. Eldar and M. B. Elowitz, Nature **467**, 167 (2010).
[19] G. Balázsi, A. van Oudenaarden, and J. J. Collins, Cell **144**, 910 (2011).
[20] B. Munsky, G. Neuert, and A. van Oudenaarden, Science **336**, 183 (2012).
[21] R. Alves and M. A. Savageau, Mol. Microbiol. **48**, 25 (2003).
[22] A. Bandyopadhyay and S. K. Banik, Biosystems **110**, 107 (2012).
[23] O. A. Igoshin, R. Alves, and M. A. Savageau, Mol. Microbiol. **68**, 1196 (2008).
[24] T. Miyashiro and M. Goulian, Proc. Natl. Acad. Sci. USA **105**, 17457 (2008).
[25] A. M. Kierzek, L. Zhou, and B. L. Wanner, Mol. Biosyst. **6**, 531 (2010).
[26] R. B. Hoyle, D. Avitabile, and A. M. Kierzek, PLoS Comput. Biol. **8**, e1002396 (2012).
[27] M. Samoilov, S. Plyasunov, and A. P. Arkin, Proc. Natl. Acad. Sci. USA **102**, 2310 (2005).
[28] A. Goldbeter and D. E. Koshland, Proc. Natl. Acad. Sci. USA **78**, 6840 (1981).
[29] A. Goldbeter and D. E. Koshland, Q. Rev. Biophys. **15**, 555 (1982).
[30] S. Tănase-Nicola, P. B. Warren, and P. R. ten Wolde, Phys. Rev. Lett. **97**, 068102 (2006).
[31] M. L. Simpson, C. D. Cox, and G. S. Sayler, J. Theor. Biol. **229**, 383 (2004).
[32] T. Shibata and K. Fujimoto, Proc. Natl. Acad. Sci. USA **102**, 331 (2005).
[33] N. G. van Kampen, *Stochastic Processes in Physics and Chemistry* (North-Holland, Amsterdam, 2005).
[34] J. Elf and M. Ehrenberg, Genome Res. **13**, 2475 (2003).
[35] P. Mehta, S. Goyal, and N. S. Wingreen, Mol. Syst. Biol. **4**, 221 (2008).
[36] P. S. Swain, J. Mol. Biol. **344**, 965 (2004).
[37] D. T. Gillespie, J. Comput. Phys. **22**, 403 (1976).
[38] D. T. Gillespie, J. Phys. Chem. **81**, 2340 (1977).
[39] D. Nevozhay, R. M. Adams, K. F. Murphy, K. Josic, and G. Balázsi, Proc. Natl. Acad. Sci. USA **106**, 5123 (2009).
[40] U. Fano, Phys. Rev. **72**, 26 (1947).
[41] C. E. Shannon, Bell Syst. Tech. J. **27**, 379 (1948).
[42] A. Borst and F. E. Theunissen, Nat. Neurosci. **2**, 947 (1999).
[43] R. Cheong, A. Rhee, C. J. Wang, I. Nemenman, and A. Levchenko, Science **334**, 354 (2011).
[44] C. G. Bowsher, M. Voliotis, and P. S. Swain, PLoS Comput. Biol. **9**, e1002965 (2013).